



Improving rate performance of cathode material $\text{Li}_{1.2}\text{Mn}_{0.54}\text{Co}_{0.13}\text{Ni}_{0.13}\text{O}_2$ via niobium doping

Li Zhao¹ · Qing Wu¹ · Jinzhu Wu¹

Received: 13 November 2017 / Revised: 30 January 2018 / Accepted: 5 February 2018 / Published online: 22 February 2018
© Springer-Verlag GmbH Germany, part of Springer Nature 2018

Abstract

As a promising Li-ion battery cathode active material, lithium-rich manganese-based layer-structured oxides suffer from inferior cycle performance and poor rate capability. Herein, Nb-doped $\text{Li}_{1.2}\text{Mn}_{0.54}\text{Ni}_{0.13}\text{Co}_{0.13}\text{O}_2$ is prepared by a sol-gel method, and the effects of Nb doping on its electrochemical performance are investigated. It is concluded that the Nb-doped $\text{Li}_{1.2}\text{Mn}_{0.54}\text{Ni}_{0.13}\text{Co}_{0.13}\text{O}_2$ has a good layered structure along *c*-axis independent on the amount of Nb dopant and little cationic mixing. Nb doping for $\text{Li}_{1.2}\text{Mn}_{0.54}\text{Ni}_{0.13}\text{Co}_{0.13}\text{O}_2$ has no obvious influence on its morphology. It is found that Nb doping can enhance the electrochemical activity of $\text{Li}_{1.2}\text{Mn}_{0.54}\text{Ni}_{0.13}\text{Co}_{0.13}\text{O}_2$, such as improved rate performance and cycle performance under high rate conditions. $\text{Li}_{1.2}\text{Mn}_{0.54}\text{Ni}_{0.13}\text{Co}_{0.13}\text{O}_2$ doped with 0.015 Nb shows the best cycle performance under the high rate with the capacity maintenance of 95.4% after 100 cycles under 5 C rate, which is higher than that of the undoped one by 10.5%.

Keywords Sol-gel method · Doping · Niobium · Li-ion battery · Cathode material

Introduction

With the development of electric vehicles (EV), lithium ion batteries are regarded as the best power sources for EV [1, 2]. However, the current Li-ion battery technology cannot fully meet the demands of EV application yet due to its low energy density and power density. Performance of Li-ion batteries crucially depends on the positive electrode material used, so the preparation of the positive electrode materials with high power density, high capacity [3–6], low price, and good stability becomes the current research direction [7–11]. Li-rich layered oxides have been identified as the most promising candidate for EV. These materials provide $\geq 250 \text{ mAh g}^{-1}$ reversible capacities by applying a high charging voltage [12–16], whereas conventional layered cathodes only have reversible capacities of 140–190 mAh g^{-1} [17, 18].

Li-rich cathode materials with general formula $x\text{LiMO}_2 \cdot (1-x)\text{Li}_2\text{MnO}_3$ (where M = Mn, Co, Ni, etc) have generated lots of research interest due to their large capacity and

complex crystal structure [19–23]. Li-rich phase $\text{Li}_{1.2}\text{Ni}_{0.13}\text{Co}_{0.13}\text{Mn}_{0.54}\text{O}_2$ which can be considered as composite of $\text{LiNi}_{0.33}\text{Co}_{0.33}\text{Mn}_{0.33}\text{O}_2$ and Li_2MnO_3 is the most studied member of the family because of its high stable capacity [24–26].

Though Li-rich layered oxides exhibit almost double the capacity of well-known cathode materials like LiCoO_2 , LiFePO_4 , or LiMn_2O_4 , however, there are several problems that seriously limit their practical application. For example, oxygen evolution during the first charge in the high voltage region results in the first cycle large initial irreversible capacity loss, rapidly decreased capacity, and poor rate performance results from layered to spinel conversion during long-term cycling [27–31]. Several strategies were performed to improve rate capability and cycling stability of Li-rich layered oxide, such as surface coating [32–35], bulk doping [36–39], core-shell structure [40, 41], and synthesis of nanostructured material [42, 43].

Among these methods, element doping has been proved to be a simple and effective approach to improve the electrochemical performance of Li-rich cathode materials. Many elements have been extensively used as doping materials. It was reported that K^+ doping in $\text{Li}_{1.2}\text{Mn}_{0.54}\text{Co}_{0.13}\text{Ni}_{0.13}\text{O}_2$ oxide effectively alleviated layered-spinel intergrowth and stabilized the host layered structure with significantly improved cycling performance [44]. The replacement of Li with Mg for

✉ Li Zhao
dhx907@hit.edu.cn

¹ School of Chemistry and Chemical Engineering, Harbin Institute of Technology, Harbin 150001, China

$\text{Li}_{1.2}\text{Mn}_{0.54}\text{Ni}_{0.13}\text{Co}_{0.13}\text{O}_2$ cathode showed enhanced specific capacity, rate capability, and cyclic stability [45]. Xin Feng reported that Ti-doped $\text{Li}_{1.2}\text{Mn}_{0.54}\text{Co}_{0.13}\text{Ni}_{0.13}\text{O}_2$ exhibits an initial capacity of 320 mAh g^{-1} and a capacity retention of 71% after 300 cycles as well as good rate performance. These improvements are attributed to the Ti doping-induced enhancement in conductivity, diffusion, activation energy of Mn migration, and Ti-O bonding [46]. To improve the rate performance and decelerate the voltage decay of Li-rich layered oxide cathode materials, Se element was doped in Li-rich materials. Se doping can improve the degree of crystallinity of Li_2MnO_3 and effectively improve the rate capability and decelerate the voltage decay process of these cathode materials during cycling via suppressing the oxidation process of O^{2-} to O_2 and curbing a layered-to-spinel phase transformation [47]. Li-rich layered materials with B-doped exhibit excellent cycling performance and voltage stability. After 51 cycles at 0.2 C, boron incorporated material can deliver 211 mAh g^{-1} with a capacity retention of 89.9% [48]. Li-rich layered oxide by annealing the acid-treated cathode powder with a Ga source to allow the Ga doping into the lattice reduced the voltage depression in the cycled electrode [49]. Li-rich layered oxides with gradient polyanion doping show a high reversible discharge capacity of $\approx 300 \text{ mAh g}^{-1}$ at 0.1 C, excellent cycling stability with a capacity retention of 95% after 100 cycles, and enhanced electrode kinetics [50].

In this work, Li-rich material $\text{Li}_{1.2}\text{Mn}_{0.54}\text{Ni}_{0.13}\text{Co}_{0.13}\text{O}_2$, which doped with different amounts of Nb, was prepared by a sol-gel method. The effects of doped Nb on the structure and electrochemical performance of the materials were investigated. Two factors were considered to adopt niobium as dopant: ion radius and valence. The radius of niobium ion is bigger than that of manganese ion, and the valence of niobium ion is higher than that of manganese ion. So the doping of niobium in $\text{Li}_{1.2}\text{Mn}_{0.54}\text{Co}_{0.13}\text{Ni}_{0.13}\text{O}_2$ would enlarge the interlayer spacing and improve the electroconductivity. All these change will be benefit to rate performance of materials..

Experimental

Preparation of materials

All the chemicals used in this work were of analytical grade and with no further purification. The cathode material $\text{Li}_{1.2}\text{Mn}_{0.54-x}\text{Ni}_{0.13}\text{Co}_{0.13}\text{Nb}_x\text{O}_2$ was synthesized by sol-gel method. A stoichiometric amount of $\text{Ni}(\text{CH}_3\text{COO})_2 \cdot 4\text{H}_2\text{O}$, $\text{Co}(\text{CH}_3\text{COO})_2 \cdot 4\text{H}_2\text{O}$, $\text{Mn}(\text{CH}_3\text{COO})_2 \cdot 4\text{H}_2\text{O}$, and $\text{LiCH}_3\text{COO} \cdot \text{H}_2\text{O}$ was dissolved in distilled water with 5% excess of LiCH_3COO , the solution was labeled as A. Amount of glycolic acid was dissolved in 20-mL distilled water, and the solution was labeled as B. The mole ratio of glycolic acid to all the metal ions was 1.1. Solution B was

dropwise added into the stirring solution A, and the pH value of the solution was adjusted to 7.5 using ammonia water. Thereafter, the solution was evaporated under continuous stirring at 90°C until the viscosity maroon aquagel was formed. After drying at 120°C in a drying oven overnight, the xerogel was crushed, subsequently heated at 450°C for 5 h in air to decompose the organic constituents and acetate components. The sample was then grounded and pelletized, and a amount of Nb_2O_5 was added in the sample. The mixture was grounded for 1 h and calcined at 900°C for 12 h followed by grounding for later use as the temperature cooled down to room temperature.

Performance measurements

All the samples were characterized using X-ray diffraction (XRD; Rigaku Ultima D/max-RB 12 KW) with a $\text{Cu K}\alpha$ radiation source. Data was collected in the range $10\text{--}90^\circ$ at a scanning rate of 5° min^{-1} . The chemical composition of samples was measured quantitatively by inductively coupled plasma atomic emission spectrometry (ICP-AES, ICPE 9000 Shimadzu). The surface morphologies and microstructures of the samples were observed using a Hitachi SU8010 scanning electron microscope (SEM).

The electrochemical properties of the samples were examined in the CR2025 coin type cells. The cathode electrodes were prepared as follow: the sample: acetylene black: PVDF = 8:1:1 with an appropriate amount of *N*-methyl-2-pyrrolidone (NMP) ground to a uniform slurry substance. The obtained slurry was coated on the surface of aluminum foil and dried in a vacuum oven at 50°C for 10 h and then formed into electrode sheets. The mass of active material in the electrode for final cell assembly is 1.5 mg cm^{-2} , and the thickness of the electrode is about $10 \mu\text{m}$. The CR2025 button cells were fabricated by using Li metal as the negative electrode and the prepared electrode sheet as positive electrode in an argon-filled glove box. The electrolyte solution was a 1 mol L^{-1} LiPF_6 . The galvanostatic charge-discharge tests were performed on a BTS series battery testing system which is made by Neware Technology between 2.0 and 4.8 V at room temperature.

A CHI430 electrochemical workstation which is made by CH Instruments Inc. was used to perform cyclic voltammograms (CV) of the prepared materials between 2.0 and 4.8 V at a sweep rate of 0.1 mV s^{-1} at room temperature. The electrochemical impedance spectroscopy (EIS) measurements were conducted by a M2273 electrochemical measurement system which is made by the EG&G company at room temperature. A two-electrode system was used to conduct the EIS of the cells at frequencies from 10 MHz to 0.01 Hz with an AC perturbation signal of 5 mV. All the cells were discharged to 2.0 V at 0.1 C and relaxed for another 2 h before the EIS measurement.

The potentials throughout the paper are referenced to the Li^+/Li couple.

Results and discussion

Figure 1 shows XRD patterns of different $\text{Li}_{1.2}\text{Mn}_{0.54-x}\text{Co}_{0.13}\text{Ni}_{0.13}\text{Nb}_x\text{O}_2$. As can be seen, all the diffraction peaks are sharp, indicating that $\text{Li}_{1.2}\text{Mn}_{0.54-x}\text{Co}_{0.13}\text{Ni}_{0.13}\text{Nb}_x\text{O}_2$ ($x = 0, 0.01, 0.015, \text{ and } 0.02$) have a good crystallinity. The well-separated diffraction peaks of (006)/(012) and (108)/(110) demonstrate a pure layer structure [51], and the corresponding lattice parameters are calculated and presented in Table 1.

All the diffraction peaks can be indexed to $\alpha\text{-NaFeO}_2$ (PDF no. 20-1115), indicating that the as-prepared $\text{Li}_{1.2}\text{Mn}_{0.54-x}\text{Co}_{0.13}\text{Ni}_{0.13}\text{Nb}_x\text{O}_2$ have a $\alpha\text{-NaFeO}_2$ structure with $R\bar{3}m$ space group. Besides, the well-separated diffraction peaks of (006)/(012) and (108)/(110) demonstrate their layered structure [51]. Generally, the value of c/a and $I_{(003)}/I_{(104)}$ is indicative of the ordering and the cationic mixing degree of the layered structure [52, 53], a higher value of $I_{(003)}/I_{(104)}$ indicates better ordering for the cation [54]. From Table 1, all $\text{Li}_{1.2}\text{Mn}_{0.54-x}\text{Co}_{0.13}\text{Ni}_{0.13}\text{Nb}_x\text{O}_2$ have a good layered structure since the c/a values of were all larger than 4.899. The $I_{(003)}/I_{(104)}$ values of all $\text{Li}_{1.2}\text{Mn}_{0.54-x}\text{Co}_{0.13}\text{Ni}_{0.13}\text{Nb}_x\text{O}_2$ were greater than 1.2, meaning little cationic mixing, among $\text{Li}_{1.2}\text{Mn}_{0.525}\text{Co}_{0.13}\text{Ni}_{0.13}\text{Nb}_{0.015}\text{O}_2$ has the least cationic mixing. The c value represents the distance between Li_2O layer and MO layer. The c values of different $\text{Li}_{1.2}\text{Mn}_{0.54-x}\text{Co}_{0.13}\text{Ni}_{0.13}\text{Nb}_x\text{O}_2$ change slightly with increasing the amount of Nb dopant, and $\text{Li}_{1.2}\text{Mn}_{0.52}\text{Co}_{0.13}\text{Ni}_{0.13}\text{Nb}_{0.02}\text{O}_2$ has a larger distance between Li_2O layer and MO layer, leading to easier intercalation of Li-ions and resulting a higher discharge capacity. Dahn [55] found that the lower the R factor ($R = (I_{(006)} + I_{(012)})/I_{(101)}$), the higher the order of the material

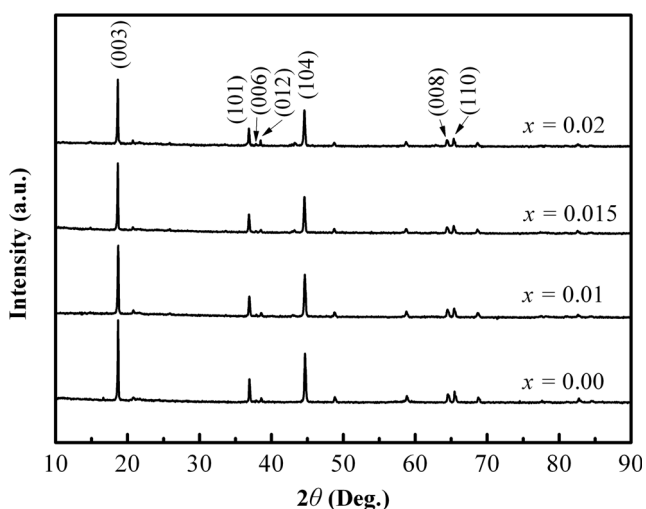


Fig. 1 XRD patterns of $\text{Li}_{1.2}\text{Mn}_{0.54-x}\text{Co}_{0.13}\text{Ni}_{0.13}\text{Nb}_x\text{O}_2$ materials

Table 1 Lattice parameters of $\text{Li}_{1.2}\text{Mn}_{0.54-x}\text{Co}_{0.13}\text{Ni}_{0.13}\text{Nb}_x\text{O}_2$ materials

x	a (Å)	c (Å)	c/a ratio	$I_{(003)}/I_{(104)}$	R
0	2.849	14.229	4.995	1.640	0.267
0.01	2.851	14.233	4.992	1.428	0.324
0.015	2.853	14.247	4.993	1.710	0.237
0.02	2.853	14.251	4.994	1.644	0.279

which possesses better electrochemical performance. From Table 1, $\text{Li}_{1.2}\text{Mn}_{0.525}\text{Co}_{0.13}\text{Ni}_{0.13}\text{Nb}_{0.015}\text{O}_2$ has the least R value, which means that its electrochemical performance may be the best.

The chemical compositions of the samples were confirmed by the ICP elemental analysis technique. As presented in Table 2, the results indicate that the average chemical compositions of the as-synthesized materials are very close to the targeted stoichiometry.

The morphologies and sizes of the samples have effects on their electrochemical performance. Figure 2 shows SEM images of different $\text{Li}_{1.2}\text{Mn}_{0.54-x}\text{Co}_{0.13}\text{Ni}_{0.13}\text{Nb}_x\text{O}_2$. As displayed in Fig. 2, all $\text{Li}_{1.2}\text{Mn}_{0.54-x}\text{Co}_{0.13}\text{Ni}_{0.13}\text{Nb}_x\text{O}_2$ show a similar morphology with the sizes of 200–400 nm. It can be seen that the amounts of Nb dopant have little influence on the sizes of material. For nanomaterials, since the diffusion path for the Li-ions' migration can be greatly reduced, rate performance can be improved. Figure 2e indicates that niobium was evenly distributed in the host material.

Figure 3 shows the first charge and discharge curve of different $\text{Li}_{1.2}\text{Mn}_{0.54-x}\text{Co}_{0.13}\text{Ni}_{0.13}\text{Nb}_x\text{O}_2$. It can be seen that the first discharge capacity of the Nb-doped material is increased, for example, the first discharge capacity of $\text{Li}_{1.2}\text{Mn}_{0.53}\text{Co}_{0.13}\text{Ni}_{0.13}\text{Nb}_{0.01}\text{O}_2$ is the highest, and the first charge and discharge efficiency of $\text{Li}_{1.2}\text{Mn}_{0.525}\text{Co}_{0.13}\text{Ni}_{0.13}\text{Nb}_{0.015}\text{O}_2$ is 68.3% which is 69.1% of that of the undoped one. With the increase of the Nb doping amount, the first charge and discharge efficiency is gradually reduced.

Figure 4 shows the cycle performance of different $\text{Li}_{1.2}\text{Mn}_{0.54-x}\text{Co}_{0.13}\text{Ni}_{0.13}\text{Nb}_x\text{O}_2$ materials. It can be seen from Fig. 4a that the first discharge capacity of the Nb-doped $\text{Li}_{1.2}\text{Mn}_{0.54-x}\text{Co}_{0.13}\text{Ni}_{0.13}\text{Nb}_x\text{O}_2$ was decreased at 0.2 C in comparison to the undoped one with the capacity retention rates of 69.8% (0.00 Nb), 87.1% (0.01 Nb), 88.9% (0.015 Nb), and 83.0% (0.02 Nb) after 50 cycles, respectively. From Fig. 4b, it could be seen that the capacity of $\text{Li}_{1.2}\text{Mn}_{0.525}\text{Co}_{0.13}\text{Ni}_{0.13}\text{Nb}_{0.015}\text{O}_2$ is 146.3 mAh g^{-1} after 100 cycles, and its capacity retention rate is 99.1%, which is higher than 91.7% of the undoped one. It can be seen from Fig. 4c that the discharge capacity of Nb-doped $\text{Li}_{1.2}\text{Mn}_{0.54-x}\text{Co}_{0.13}\text{Ni}_{0.13}\text{Nb}_x\text{O}_2$ is slightly increased at 5 C compared with the undoped one, for example, and the discharge capacity of

Table 2 Chemical composition results of ICP analysis of $\text{Li}_{1.2}\text{Mn}_{0.54-x}\text{Co}_{0.13}\text{Ni}_{0.13}\text{Nb}_x\text{O}_2$ materials. Numbers in parentheses indicate designed values

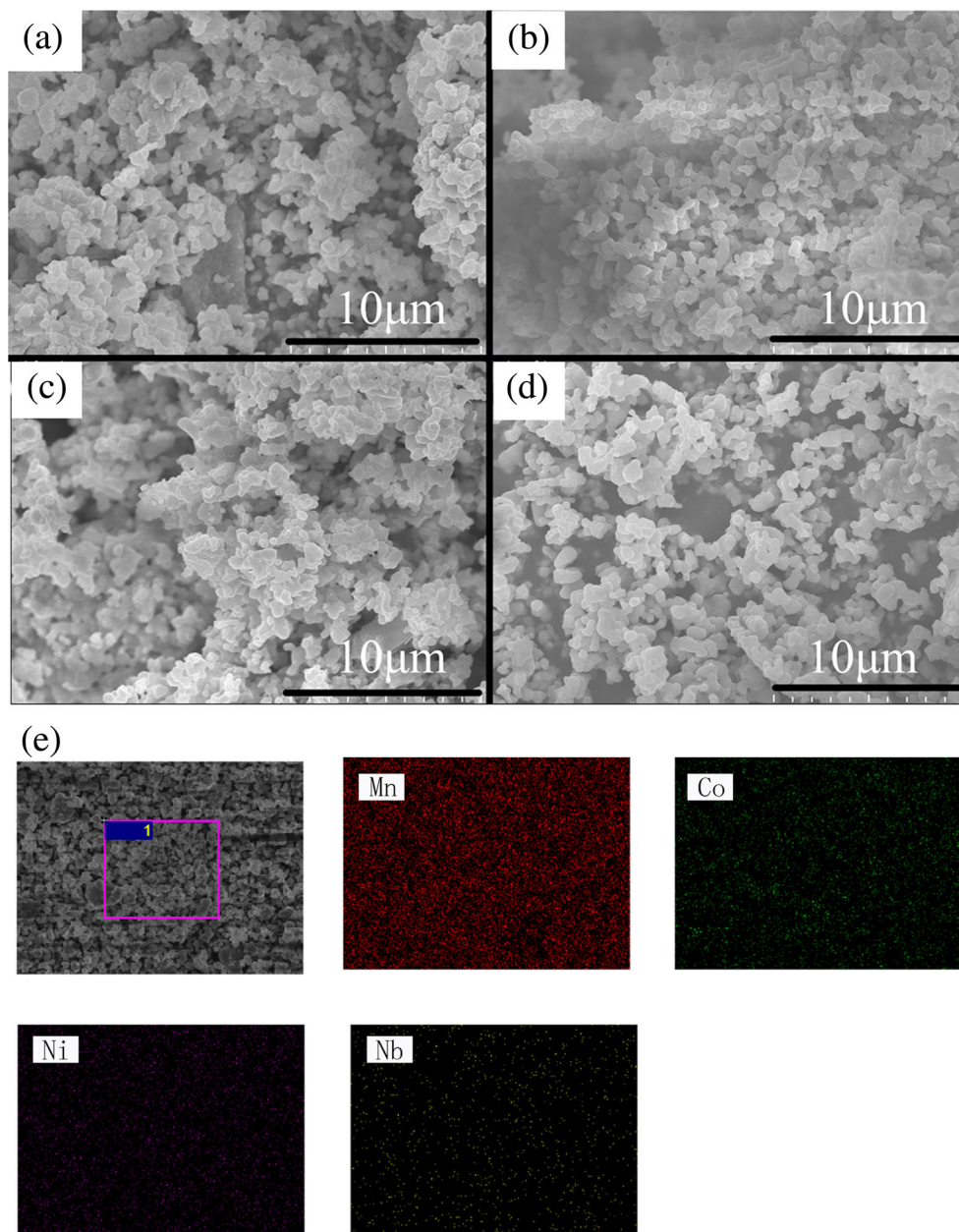
Metal ions	$x = 0$	$x = 0.01$	$x = 0.015$	$x = 0.02$
Li	1.191 (1.200)	1.193 (1.200)	1.192 (1.200)	1.195 (1.200)
Mn	0.545 (0.540)	0.536 (0.530)	0.527 (0.525)	0.516 (0.520)
Ni	0.133 (0.130)	0.129 (0.130)	0.128 (0.130)	0.127 (0.130)
Co	0.129 (0.130)	0.128 (0.130)	0.132 (0.130)	0.134 (0.130)
Nb	0 (0)	0.009 (0.010)	0.013 (0.015)	0.022 (0.020)

$\text{Li}_{1.2}\text{Mn}_{0.525}\text{Co}_{0.13}\text{Ni}_{0.13}\text{Nb}_{0.015}\text{O}_2$ is 95.0 mAh g^{-1} at 5 C. From the cycle performance, 0.015 Nb doping can improve the cycle performance of $\text{Li}_{1.2}\text{Mn}_{0.54}\text{Co}_{0.13}\text{Ni}_{0.13}\text{O}_2$.

The rate performance of different $\text{Li}_{1.2}\text{Mn}_{0.54-x}\text{Co}_{0.13}\text{Ni}_{0.13}\text{Nb}_x\text{O}_2$ is shown in Fig. 5. The rate

performance of Nb doped material is improved over the undoped one. At the discharge rate of 5 C, the discharge capacity of the doped material is 95.0 mAh g^{-1} , which is higher than 70.0 mAh g^{-1} for the undoped one. Nb doping for the lithium-rich materials could improve the cycle

Fig. 2 SEM images of $\text{Li}_{1.2}\text{Mn}_{0.54-x}\text{Co}_{0.13}\text{Ni}_{0.13}\text{Nb}_x\text{O}_2$ material. **a** $x = 0$. **b** $x = 0.01$. **c** $x = 0.015$. **d** $x = 0.02$. **e** EDS element mapping of sample



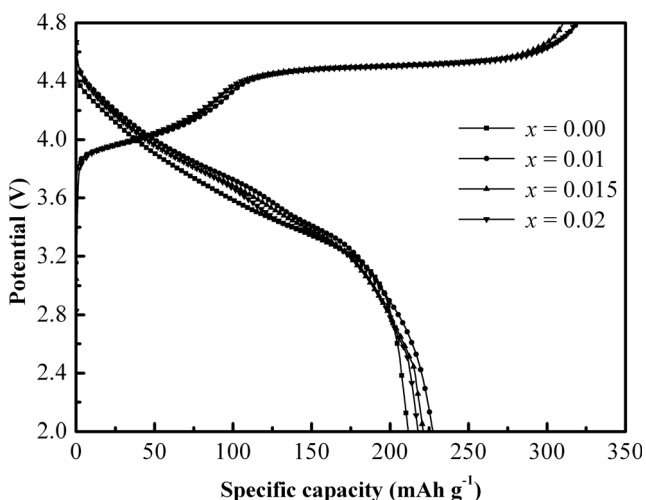


Fig. 3 Initial charge and discharge profiles of $\text{Li}_{1.2}\text{Mn}_{0.54-x}\text{Co}_{0.13}\text{Ni}_{0.13}\text{Nb}_x\text{O}_2$ materials

performance, while the rate performance has also been improved.

To explore the electrochemical redox responses of different $\text{Li}_{1.2}\text{Mn}_{0.54-x}\text{Co}_{0.13}\text{Ni}_{0.13}\text{Nb}_x\text{O}_2$ electrodes, CV measurement was carried out. As shown in Fig. 6, in initial anodic process, all the cathode electrodes have two obvious anodic peaks around at 4.2 and 4.6 V. The oxidation peak at 4.2 V corresponds to the ionization of lithium ions from the LiMO_2 ($M = \text{Mn, Ni, Co}$) structure, accompanied by the oxidation of Ni^{2+} to Ni^{4+} and Co^{3+} to Co^{4+} , which correspond to the first discharge platform in the first charge-discharge curve. The oxidation peak at 4.6 V corresponds to the activation of Li_2MnO_3 , corresponding to the second discharge platform in the first charge-discharge curve. When the Li_2MnO_3 component in the lithium-rich material is charged to 4.4 V and above,

Fig. 4 Cycling performance of $\text{Li}_{1.2}\text{Mn}_{0.54-x}\text{Co}_{0.13}\text{Ni}_{0.13}\text{Nb}_x\text{O}_2$ materials. **a** 0.2 C. **b** 1 C. **c** 5 C

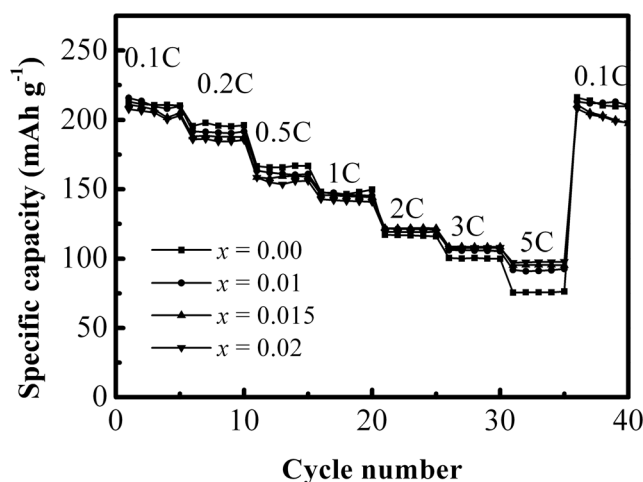
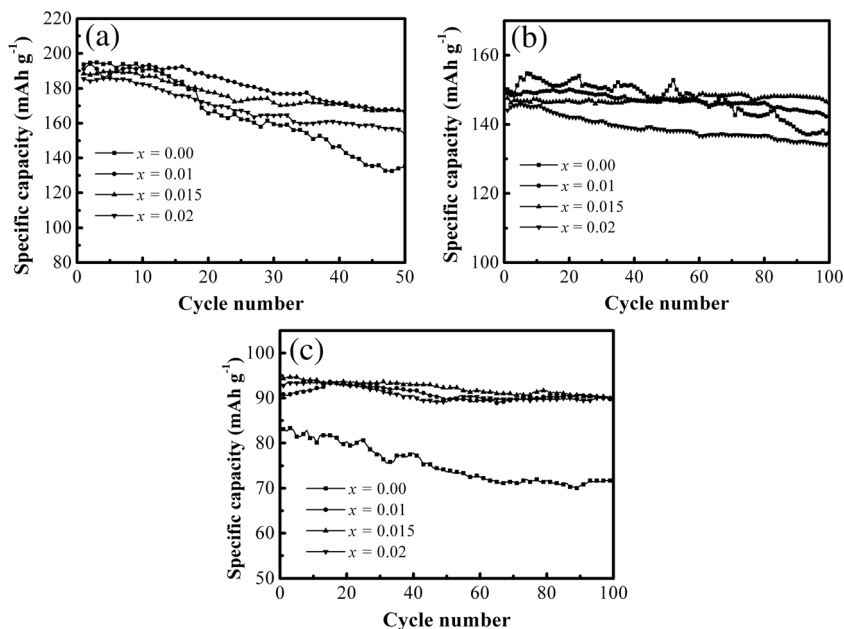
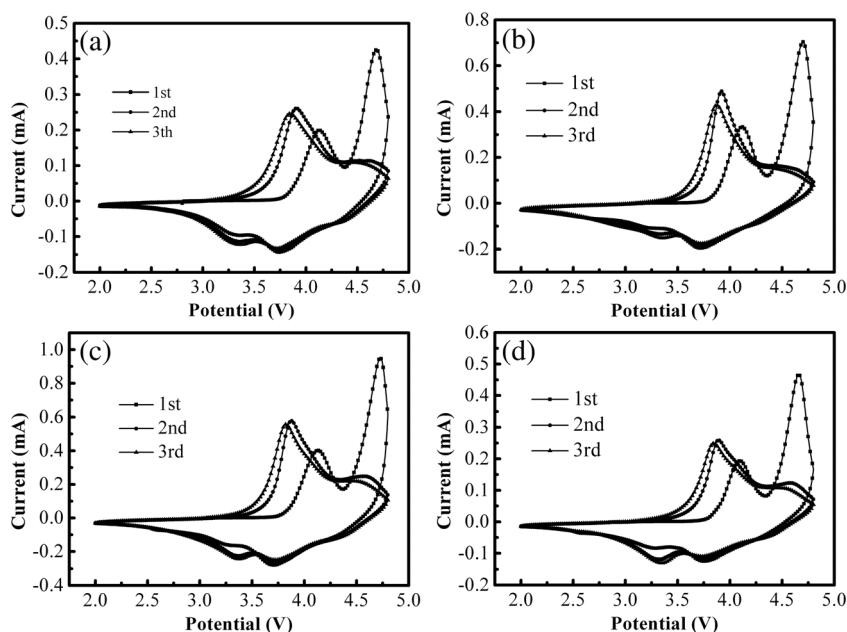


Fig. 5 Rate performance of $\text{Li}_{1.2}\text{Mn}_{0.54-x}\text{Co}_{0.13}\text{Ni}_{0.13}\text{Nb}_x\text{O}_2$ materials

Li will be removed from Li_2MnO_3 , accompanied by the loss of oxygen and the generation of MnO_2 component, which is irreversible with a large irreversible capacity and thus lead to the disappearance of the second anodic peak during the following two scanning laps. In addition, a negative shift of the oxidation peak potential was observed, which becomes decreased with the increase of scanning number, illustrating a good reversibility of the cathodes. With the increase of Nb content, the oxidation peak at 4.6 V in the first cycle curve gradually increases, which corresponds to the gradual decrease of the first charge and discharge efficiency. The reduction peaks at about 3.25 V became increased with the increase of the Nb-doping amount, and they coincide each other during the second and third lap. The reduction peaks are more obvious in the second and third cycle curves, indicating that the cathode material was further activated. These findings are

Fig. 6 CV curves of $\text{Li}_{1.2}\text{Mn}_{0.54-x}\text{Co}_{0.13}\text{Ni}_{0.13}\text{Nb}_x\text{O}_2$ materials. **a** $x = 0.00$. **b** $x = 0.01$. **c** $x = 0.015$. **d** $x = 0.02$



consistent with those in the initial charge-discharge curves of the samples.

In order to study the kinetics of lithium ion intercalation/deintercalation of lithium-rich layered materials, EIS measurements were performed. Figure 7 is the Nyquist plots of $\text{Li}_{1.2}\text{Mn}_{0.54-x}\text{Co}_{0.13}\text{Ni}_{0.13}\text{Nb}_x\text{O}_2$ materials. The impedance spectrum of the Li-rich layered material usually consists of three regions, reflecting the serial nature of the lithium ion intercalation/deintercalation process. The semicircular in high frequency region is attributed to the Li-ion transport through the surface, that in the medium-frequency region is ascribed to charge-transfer reaction at an electrolyte-electrode interface, and the low frequency region is attributed to the solid diffusion of lithium ions in the inserted compound. The high-spectrum impedance and the real part of the impedance diagram represent the ohmic resistance (R_s) of the solution. The semicircular diameter corresponds to the surface charge transfer resistance (R_{ct}), followed by a slash corresponding to the Warburg impedance of lithium ion diffusion. As can be seen from Fig. 7, the R_s of different samples could be ignored compared to R_{ct} , while R_{ct} is the smallest for $\text{Li}_{1.2}\text{Mn}_{0.525}\text{Co}_{0.13}\text{Ni}_{0.13}\text{Nb}_{0.015}\text{O}_2$. The results show that the ion transport channel of $\text{Li}_{1.2}\text{Mn}_{0.525}\text{Co}_{0.13}\text{Ni}_{0.13}\text{Nb}_{0.015}\text{O}_2$ is short, which can accelerate the Li^+ deintercalation to achieve good rate performance. The surface charge transfer resistance of $\text{Li}_{1.2}\text{Mn}_{0.525}\text{Co}_{0.13}\text{Ni}_{0.13}\text{Nb}_{0.015}\text{O}_2$ is lower than the other two materials, indicating its highest rate capability. In addition, the lithium ion diffusion coefficient (D) of samples is calculated from the inclined line in the low-frequency region and presented in Table 3. As shown in Table 3, Nb-doped materials demonstrate higher lithium ion diffusion coefficient than the undoped one, which agree well with the electrochemical results.

Conclusions

In this work, the Li-rich material $\text{Li}_{1.2}\text{Mn}_{0.54}\text{Ni}_{0.13}\text{Co}_{0.13}\text{O}_2$ doped with Nb was successfully prepared by a sol-gel method, and the effects of the Nb-doping amount on the morphology, the structure properties, and the electrochemical performance of the materials were studied. Nb doping has no significant effects on its original layered structure and cationic mixing, but slightly impacts on the stacking along c -axis. The reduction potential became increased with the increase of the Nb-doping amount, this will benefit to the discharge performance. Nb doping for $\text{Li}_{1.2}\text{Mn}_{0.54}\text{Ni}_{0.13}\text{Co}_{0.13}\text{O}_2$ can notably enhance its cycle performance, the capacity retention rates of the materials at 0.2 C was improved from 69 to 88% after 50 cycles, and $\text{Li}_{1.2}\text{Mn}_{0.525}\text{Co}_{0.13}\text{Ni}_{0.13}\text{Nb}_{0.015}\text{O}_2$ shows the best high rate cycle performance with the capacity maintenance of 95.4% after 100 cycles under 5 C rate, which is higher than that of

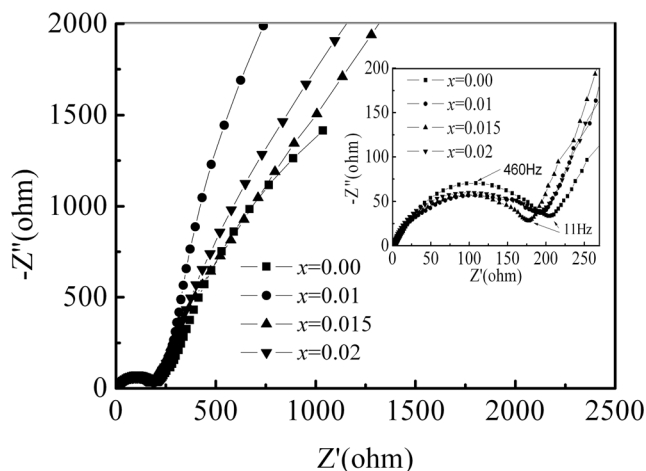


Fig. 7 Nyquist plots of $\text{Li}_{1.2}\text{Mn}_{0.54-x}\text{Co}_{0.13}\text{Ni}_{0.13}\text{Nb}_x\text{O}_2$ materials

Table 3 Diffusion coefficient of $\text{Li}_{1.2}\text{Mn}_{0.54-x}\text{Co}_{0.13}\text{Ni}_{0.13}\text{Nb}_x\text{O}_2$ materials

x	0	0.01	0.015	0.02
D ($\text{cm}^2 \text{s}^{-1}$) $\times 10^{-15}$	0.32	5.51	3.52	3.23

the undoped one by 10.5%. The rate performance of Nb doped material is also improved over the undoped one. At the discharge rate of 5 C, the discharge specific capacity of the doped material is 95.0 mAh g^{-1} , which is higher than 70.0 mAh g^{-1} for the undoped one.

Funding information This work was supported by the Shenzhen EPT Battery Co., Ltd.

References

- Kumar PS, Sakunthala A, Reddy MV, Shanmugam S, Prabu M (2016) Correlation between the structural, electrical and electrochemical performance of layered $\text{Li}(\text{Ni}_{0.33}\text{Co}_{0.33}\text{Mn}_{0.33})\text{O}_2$ for lithium ion battery. *J SolidState Electrochem* 20(7):1865–1876
- Kong JZ, Zhai HF, Ren C, Tai GA, Yang XY, Zhou F, Li H, Li JX, Tang Z (2014) High-capacity $\text{Li}(\text{Ni}_{0.5}\text{Co}_{0.2}\text{Mn}_{0.3})\text{O}_2$ lithium-ion battery cathode synthesized using a green chelating agent. *J SolidState Electrochem* 18(1):181–188
- Zhang R, Wang XY, Wei SY, Wang X, Liu M, Hu H (2017) Iron fluoride microspheres by titanium dioxide surface modification as high capacity cathode of Li-ion batteries. *J Alloys Compd* 719:331–340
- Opra DP, Gnedenkov SV, Sokolov AA, Podgorbunsky AB, Laptash NM, Sinebryukhov SL (2015) Fluorine substituted molybdenum oxide as cathode material for Li-ion battery. *Mater Lett* 160:175–178
- Zeng QC, Li Y, Wu KH, Huang N, Dalapati S, Su BJ, Jang LY, Gentle IR, Jiang DL, Wang DW (2018) Long-chain solid organic polysulfide cathode for high-capacity secondary lithium batteries. *Energy Storage Mater* 12:30–36
- Kuang Q, Zhao YM, Dong YZ, Fan QH (2015) Sol-gel synthesized zirconium pyrovanadate as a high-capacity cathode for rechargeable Li batteries. *Electrochim Acta* 170:229–233
- Zhong H, Sun M, Li Y, He J, Yang J, Zhang L (2016) The polyacrylic latex: an efficient water-soluble binder for $\text{LiNi}_{1/3}\text{Co}_{1/3}\text{Mn}_{1/3}\text{O}_2$ cathode in li-ion batteries. *JSolidState Electrochem* 20(1):1–8
- Gangulibabu Bhuvanewari D, Kalaiselvi N (2013) Comparison of corn starch-assisted sol-gel and combustion methods to prepare $\text{LiMn}_x\text{Co}_y\text{Ni}_z\text{O}_2$ compounds. *J SolidState Electrochem* 17(1):9–17
- Wang L, Li J, He X, Pu W, Wan C, Jiang C (2009) Recent advances in layered $\text{LiNi}_x\text{Co}_y\text{Mn}_{1-x-y}\text{O}_2$ cathode materials for lithium ion batteries. *JSolidState Electrochem* 13(8):1157–1164
- Dou S, Wang W (2011) Synthesis and electrochemical properties of layered $\text{LiNi}_{0.5-x}\text{Mn}_{0.5-x}\text{Co}_{2x}\text{O}_2$ for lithium-ion battery from nickel manganese cobalt oxide precursor. *JSolidState Electrochem* 15(2):399–404
- Bhuvanewari D, Gangulibabu Kalaiselvi N (2012) Surfactant-coassisted sol-gel synthesis to prepare $\text{LiNi}_y\text{Mn}_y\text{Co}_{1-2y}\text{O}_2$ with improved electrochemical behavior. *JSolidState Electrochem* 16(11):3667–3674
- Zhao TL, Chen S, Li L, Zhang XF, Chen RJ, Belharouak L, Wu F, Amine K (2013) Synthesis, characterization, and electrochemistry of cathode material $\text{Li}[\text{Li}_{0.2}\text{Co}_{0.13}\text{Ni}_{0.13}\text{Mn}_{0.54}]\text{O}_2$ using organic chelating agents for lithium-ion batteries. *J Power Sources* 228:206–213
- Laisa CP, Kumar AKN, Chandrasekaran SS, Murugan P, Lakshminarasimhan N, Govindaraj R, Ramesha K (2016) A comparative study on electrochemical cycling stability of lithium rich layered cathode materials $\text{Li}_{1.2}\text{Ni}_{0.13}\text{M}_{0.13}\text{Mn}_{0.54}\text{O}_2$ where M = Fe or Co. *J Power Sources* 324:462–474
- Wang M, Luo M, Chen YB, Chen L, Yan S, Ren YZ, Chu M (2017) A new approach to improve the electrochemical performance of Li rich cathode material by precursor pretreatment. *J Alloys Compd* 696:891–899
- Li JL, Jia TK, Liu K, Zhao JW, Chen J, Cao CB (2016) Facile design and synthesis of Li-rich nanoplates cathodes with habit tuned crystal for lithium ion batteries. *J Power Sources* 333:37–42
- Zhu ZY, Cai FY, Yu J (2016) Improvement of electrochemical performance for AlF_3 -coated $\text{Li}_{1.3}\text{Mn}_{4/6}\text{Ni}_{1/6}\text{Co}_{1/6}\text{O}_{2.40}$ cathode materials for Li-ion batteries. *Ionics* 22(8):1353–1359
- Wang LN, Zhang ZG, Zhang KL (2007) A simple, cheap soft synthesis routine for LiFePO_4 using iron(III) raw material. *J Power Sources* 167(1):200–205
- Armstrong AR, Holzapfel M, Novak P, Johnson CS, Kang SH, Thackeray MM, Bruce PG (2006) Demonstrating oxygen loss and associated structural reorganization in the lithium battery cathode $\text{Li}[\text{Ni}_{0.2}\text{Li}_{0.2}\text{Mn}_{0.6}]\text{O}_2$. *J Am Chem Soc* 128(26):8694–8698
- Ma SM, Hou XH, Lin ZR, Huang YL, Gao YM, Hu SJ, Shen JD (2016) One-pot facile co-precipitation synthesis of the layered $\text{Li}_{1+x}(\text{Mn}_{0.6}\text{Ni}_{0.2}\text{Co}_{0.2})_{(1-x)}\text{O}_2$ as cathode materials with outstanding performance for lithium-ion batteries. *J SolidState Electrochem* 20(1):95–103
- Liu YJ, Wang QL, Zhang ZQ, Dou AC, Pan J, Su MR (2016) Investigation the electrochemical performance of layered cathode material $\text{Li}_{1.2}\text{Ni}_{0.2}\text{Mn}_{0.6}\text{O}_2$ coated with $\text{Li}_4\text{Ti}_5\text{O}_{12}$. *Adv Powder Technol* 27(4):1481–1487
- Chen JJ, Li ZD, Xiang HF, Wu WW, Guo X, Wu YC (2015) Bifunctional effects of carbon coating on high-capacity $\text{Li}_{1.2}\text{Ni}_{0.13}\text{Co}_{0.13}\text{Mn}_{0.54}\text{O}_2$ cathode for lithium-ion batteries. *J SolidState Electrochem* 19(4):1027–1035
- Huang X, Qiao QQ, Sun YY, Li F, Wang YL, Ye SH (2015) Preparation and electrochemical characterization of $\text{Li}(\text{Li}_{0.17}\text{Ni}_{0.2}\text{Co}_{0.05}\text{Mn}_{0.58})\text{O}_2$ coated with LiAlO_2 . *J SolidState Electrochem* 19(3):805–812
- Chen C, Geng TF, Du CY, Zuo PJ, Cheng XQ, Ma YL, Yin GP (2016) Oxygen vacancies in SnO_2 surface coating to enhance the activation of layered Li-rich $\text{Li}_{1.2}\text{Mn}_{0.54}\text{Ni}_{0.13}\text{Co}_{0.13}\text{O}_2$ cathode material for Li-ion batteries. *J Power Sources* 331:91–99
- Mohanty D, Kalnaus S, Meisner RA, Rhodes KJ, Li JL, Payzant EA, Wood DL, Daniel C (2013) Structural transformation of a lithium-rich $\text{Li}_{1.2}\text{Co}_{0.1}\text{Mn}_{0.55}\text{Ni}_{0.15}\text{O}_2$ cathode during high voltage cycling resolved by in situ X-ray diffraction. *J Power Sources* 229:239–248
- Li JG, Li JL, Yu TH, Ding FX, Xu GF, Li ZY, Zhao YG, Kang FY (2016) Stabilizing the structure and suppressing the voltage decay of $\text{Li}[\text{Li}_{0.2}\text{Mn}_{0.54}\text{Co}_{0.13}\text{Ni}_{0.13}]\text{O}_2$ cathode materials for Li-ion batteries via multifunctional Pr oxide surface modification. *Ceram Int* 42(16):18620–18630
- Koga H, Croguennec L, Mannesiez P, Menetrier M, Weill F, Bourgeois L, Duttine M, Suard E, Delmas C (2012) $\text{Li}_{1.2}\text{Mn}_{0.54}\text{Co}_{0.13}\text{Ni}_{0.13}\text{O}_2$ with different particle sizes as attractive positive electrode materials for lithium-ion batteries: insights into their structure. *J Phys Chem C* 116(25):13497–13506
- Martha SK, Nanda J, Veith GM, Dudney NJ (2012) Electrochemical and rate performance study of high-voltage lithium-rich composition: $\text{Li}_{1.2}\text{Mn}_{0.525}\text{Ni}_{0.175}\text{Co}_{0.1}\text{O}_2$. *J Power Sources* 199:220–226

28. Yu DYW, Yanagida K, Nakamura H (2010) Surface modification of Li-excess Mn-based cathode materials. *J Electrochem Soc* 157(11): A1177–A1182
29. Liu J, Manthiram A (2010) Functional surface modification of a high capacity layered $\text{Li}[\text{Li}_{0.2}\text{Mn}_{0.54}\text{Ni}_{0.13}\text{Co}_{0.13}]\text{O}_2$ cathode. *J Mater Chem* 20(19):3961–3967
30. Marom R, Amalraj SF, Leifer N, Jacob D, Aurbach D (2011) A review of advanced and practical lithium battery materials. *J Mater Chem* 21(27):9938–9954
31. Thackeray MM, Kang SH, Johnson CS, Vaughey JT, Benedek R, Hackney SA (2007) Li_2MnO_3 -stabilized LiMO_2 (M = Mn, Ni, Co) electrodes for lithium-ion batteries. *J Mater Chem* 17(30):3112–3125
32. Shi SJ, Tu JP, Tang YY, Liu XY, Zhang YQ, Wang XL, Gu CD (2013) Enhanced cycling stability of $\text{Li}[\text{Li}_{0.2}\text{Mn}_{0.54}\text{Ni}_{0.13}\text{Co}_{0.13}]\text{O}_2$ by surface modification of MgO with melting impregnation method. *Electrochim Acta* 88:671–679
33. Zhou YK, Bai PF, Tang HQ, Zhu JT, Tang ZY (2016) Chemical deposition synthesis of desirable high-rate capability Al_2O_3 -coated $\text{Li}_{1.2}\text{Mn}_{0.54}\text{Ni}_{0.13}\text{Co}_{0.13}\text{O}_2$ as a Lithium ion battery cathode material. *J Electroanal Chem* 782:256–263
34. Aida T, Tsutsui Y, Kanada S, Okada J, Hayashi K, Komukai T (2017) Ammonium tungstate modified Li-rich $\text{Li}_{1+x}\text{Ni}_{0.35}\text{Co}_{0.35}\text{Mn}_{0.30}\text{O}_2$ to improve rate capability and productivity of lithium-ion batteries. *J Solid State Electrochem* 21(7):2047–2054
35. Kong JZ, Ren C, Jiang YX, Zhou F, Yu C, Tang WP, Li H, Ye SY, Li JX (2016) Li-ion-conductive Li_2TiO_3 -coated $\text{Li}[\text{Li}_{0.2}\text{Mn}_{0.51}\text{Ni}_{0.19}\text{Co}_{0.1}]\text{O}_2$ for high-performance cathode material in lithium-ion battery. *J Solid State Electrochem* 20(5):1435–1443
36. Nayak P, Grinblat J, Levi M, Haik O, Levi E, Aurbach D (2015) Effect of Fe in suppressing the discharge voltage decay of high capacity Li-rich cathodes for Li-ion batteries. *J Solid State Electrochem* 19(9):2781–2792
37. Du J, Shan Z, Zhu K, Liu X, Tian J, Du H (2015) Improved electrochemical performance of $\text{Li}[\text{Li}_{0.2}\text{Mn}_{0.54}\text{Ni}_{0.13}\text{Co}_{0.13}]\text{O}_2$ by doping with molybdenum for Lithium battery. *J Solid State Electrochem* 19(4):1037–1044
38. Tamilarasan S, Mukherjee D, Sampath S, Natarajan S, Gopalakrishnan J (2016) Synthesis, structure and electrochemical behaviour of new Ru-containing lithium-rich layered oxides. *Solid State Ionics* 297:49–58
39. Kou YJ, Han ES, Zhu LZ, Liu LL, Zhang ZA (2016) The effect of Ti doping on electrochemical properties of $\text{Li}_{1.167}\text{Ni}_{0.4}\text{Mn}_{0.383}\text{Co}_{0.05}\text{O}_2$ for lithium-ion batteries. *Solid State Ionics* 296:154–157
40. Noh JK, Kim S, Kim H, Choi W, Chang W, Byun D, Cho BW, Chung KY (2014) Mechanochemical synthesis of Li_2MnO_3 shell/ LiMO_2 (M = Ni, Co, Mn) core-structured nanocomposites for lithium-ion batteries. *Sci Rep* 4:4847
41. Oh P, Oh SM, Li WD, Myeong S, Cho J, Manthiram A (2016) High-performance heterostructured cathodes for lithium-ion batteries with a Ni-rich layered oxide core and a Li-rich layered oxide shell. *Adv Sci* 3:1600184–1600191
42. Wang DP, Belharouak I, Zhou GW, Amine K (2013) Nanoarchitecture multi-structural cathode materials for high capacity lithium batteries. *Adv Funct Mater* 23(8):1070–1075
43. Ma DT, Li YL, Wu MS, Deng LB, Ren XZ, Zhang PX (2016) Enhanced cycling stability of Li-rich nanotube cathodes by 3D graphene hierarchical architectures for Li-ion batteries. *Acta Mater* 112:11–19
44. Li Q, Li GS, Fu CC, Luo D, Fan JM, Li LP (2014) K^+ -doped $\text{Li}_{1.2}\text{Mn}_{0.54}\text{Co}_{0.13}\text{Ni}_{0.13}\text{O}_2$: a novel cathode material with an enhanced cycling stability for lithium-ion batteries. *ACS Appl Mater Interfaces* 6(13):10330–10341
45. Xu HJ, Deng SN, Chen GH (2014) Improved electrochemical performance of $\text{Li}_{1.2}\text{Mn}_{0.54}\text{Ni}_{0.13}\text{Co}_{0.13}\text{O}_2$ by Mg doping for lithium ion battery cathode material. *J Mater Chem A* 2(36):15015–15021
46. Feng X, Gao YR, Ben LB, Yang ZZ, Wang ZX, Chen LQ (2016) Enhanced electrochemical performance of Ti-doped $\text{Li}_{1.2}\text{Mn}_{0.54}\text{Co}_{0.13}\text{Ni}_{0.13}\text{O}_2$ for lithium-ion batteries. *J Power Sources* 317:74–80
47. Ma QX, Li RH, Zheng RJ, Liu YL, Huo H, Dai CS (2016) Improving rate capability and decelerating voltage decay of Li-rich layered cathodes via selenium doping to stabilize oxygen. *J Power Sources* 331:112–121
48. Pan LC, Xia YG, Qiu B, Zhao H, Guo HC, Jia K, Gu QW, Liu ZP (2016) Structure and electrochemistry of B doped $\text{Li}(\text{Li}_{0.2}\text{Ni}_{0.13}\text{Co}_{0.13}\text{Mn}_{0.54})_{1-x}\text{B}_x\text{O}_2$ as cathode materials for lithium-ion batteries. *J Power Sources* 327:273–280
49. Song JH, Shim JH, Kapyrou A, Yeon DH, Lee DH, Kim DH, Park JH, Kang SH (2016) Suppression of voltage depression in Li-rich layered oxide by introducing GaO_4 structural units in the Li_2MnO_3 -like nano-domain. *Nano Energy* 30:717–727
50. Zhao Y, Liu JT, Wang SB, Ji R, Xia QB, Ding ZP, Wei WF, Liu Y, Wang P, Ivey DG (2016) Surface structural transition induced by gradient polyanion-doping in Li-rich layered oxides: implications for enhanced electrochemical performance. *Adv Funct Mater* 26(26):4760–4767
51. Abuzeid HAM, Hashem AMA, Abdel-Ghany AE, Eid AE, Mauger A, Groult H, Julien CM (2011) De-intercalation of $\text{Li}_x\text{Co}_{0.8}\text{Mn}_{0.2}\text{O}_2$: a magnetic approach. *J Power Sources* 196(15): 6440–6448
52. Myung ST, Kumagai N, Komaba S, Chung HT (2001) Effects of Al doping on the microstructure of LiCoO_2 cathode materials. *Solid State Ionics* 139(1–2):47–56
53. Jiao LF, Zhang M, Yuan HT, Zhao M, Guo H, Wang W, Di ZX, Wang YM (2007) Effect of Cr doping on the structural, electrochemical performance of $\text{Li}[\text{Li}_{0.2}\text{Ni}_{0.2-x/2}\text{Mn}_{0.6-x/2}\text{Cr}_x]\text{O}_2$ ($x = 0, 0.02, 0.04, 0.06, 0.08$) as cathode materials for lithium secondary batteries. *J Power Sources* 167(1):178–184
54. Sun G, Yin XC, Yang W, Song AL, Jia CX, Yang W, Du QH, Ma ZP, Shao GJ (2017) The effect of cation mixing controlled by the rmtreatment duration on the electrochemical stability of lithium transition-metal oxides. *PhysChemChemPhys* 19(44):29886–29894
55. Dahn JR, Vonsacken U, Michal CA (1990) Structure and electrochemistry of $\text{Li}_{1+x}\text{NiO}_2$ and a new Li_2NiO_2 phase with the $\text{Ni}(\text{OH})_2$ structure. *Solid State Ionics* 44(1–2):87–97